CHAPTER 5 BENDWAY-WEIR ANALYSIS

5.1 INTRODUCTION

Bendway-weir analysis was the process used to determine a HEC-RAS model that matched the flow depth and total energy loss in the physical model with bendway weirs. The HEC-RAS model was built using the Modified Test Base-line Model as a foundation.

5.2 TRIAL DEFINITIONS

A system needed to be developed in order to organize and define each variation of the bendway-weir model in HEC-RAS. Each variation of the HEC-RAS model was defined as a **Trial**. Sixteen trials were developed in an attempt to build an optimal HEC-RAS model. Trial definitions are listed in Table 5.1.

Table 5.1. Trial List

Trial Number	Description
Trial 1	Manning's n changed at all cross sections with bendway weirs, all flow rates looked at with same geometry file, **NOT** independently of each other.
Trial 2 (8 cfs)	Manning's n changed at all cross sections with bendway weirs. Flow rate, 8 cfs, has geometry file specific to the 8 cfs model run.
Trial 2 (12 cfs)	Manning's n changed at all cross sections with bendway weirs. Flow rate, 12 cfs, has geometry file specific to the 12 cfs model run.
Trial 2 (16 cfs)	Manning's n changed at all cross sections with bendway weirs. Flow rate, 16 cfs, has geometry file specific to the 16 cfs model run.
Trial 3	Contraction/Expansion coefficients only variables adjusted. Used the HEC-RAS base-line model to make adjustments to contraction and expansion coefficients for all cross sections which contained a bendway weir. Look at all flow rates with the same geometry file **NOT** independently from one another.
Trial 4 (8 cfs)	Adjust the Contraction/Expansion coefficients to the 8 cfs, Trial 2 (8 cfs) geometry file.
Trial 4 (12 cfs)	Adjust the Contraction/Expansion coefficients to the 12 cfs, Trial 2 (12 cfs) geometry file.
Trial 4 (16 cfs)	Adjust the Contraction/Expansion coefficients to the 16 cfs, Trial 2 (16 cfs) geometry file.
Trial 5 (8 cfs)	Adjust the contraction coefficients for transition section of physical model (XS8 through XS10) for the 8 cfs, Trial 4 geometry file.
Trial 5 (12 cfs)	Adjust the contraction coefficients for transition section of physical model (XS8 through XS10) for the 12 cfs, Trial 4 geometry file.
Trial 5 (16 cfs)	Adjust the contraction coefficients for transition section of physical model (XS8 through XS10) for the 16 cfs, Trial 4 geometry file.
Trial 6	Build block obstructions at each bendway-weir location in the Type III (D/S) bend. Look at all flow rates with same geometry file, **NOT** independently of one another.
Trial 7	Add ineffective flow lines to the Trial 6, HEC-RAS model upstream and downstream of each blocked structure (representing each bendway weir) to represent the dead zones and eddies between bendway weirs. Look at all flow rates with the same geometry file, **NOT** independently of one another.
Trial 8 (8 cfs)	Use Trial 7 geometry file and change Manning's n and Contraction/Expansion coefficients at all cross sections with bendway weirs. Change Manning's n specifically for 8 cfs model run.
Trial 8 (12 cfs)	Use Trial 7 geometry file and change Manning's n and Contraction/Expansion coefficients at all cross sections with bendway weirs. Change Manning's n specifically for 12 cfs model run.
Trial 8 (16 cfs)	Use Trial 7 geometry file and change Manning's n and Contraction/Expansion coefficients at all cross sections with bendway weirs. Change Manning's n specifically for 16 cfs model run.
Trial 9	Delete block obstructions from the Trial 7 geometry file and mark each weir by an ineffective flow line. Look at all flow rates with the same geometry file, **NOT** independently of one another.
Trial 10 (8 cfs)	Use Trial 8 (8 cfs) geometry file and adjust Manning's n by stations across each cross section with a bendway weir instead of adjusting Manning's n by left overbank, channel, and right overbank.

Trial Number	Description
Trial 10 (12 cfs)	Use Trial 8 (12 cfs) geometry file and adjust Manning's n by stations across each cross section with a bendway weir instead of adjusting Manning's n by left overbank, channel, and right overbank.
Trial 10 (16 cfs)	Use Trial 8 (16 cfs) geometry file and adjust Manning's n by stations across each cross section with a bendway weir instead of adjusting Manning's n by left overbank, channel, and right overbank.
Trial 11 (8 cfs)	Use Trial 8 (8 cfs) and add ineffective flow lines at the cross sections containing bendway weirs. The ineffective flow lines were added to show water passing over the high point of the bendway weir moved from the upstream eddy to the eddy downstream of the bendway weir. The flow that passes over this portion of the bendway weir is considered ineffective since it conforms to the downstream eddy.
Trial 11 (12 cfs)	Use Trial 8 (12 cfs) and add ineffective flow lines at the cross sections containing bendway weirs. The ineffective flow lines were added to show water passing over the high point of the bendway weir moved from the upstream eddy to the eddy downstream of the bendway weir. The flow that passes over this portion of the bendway weir is considered ineffective since it conforms to the downstream eddy.
Trial 11 (16 cfs)	Use Trial 8 (16 cfs) and add ineffective flow lines at the cross sections containing bendway weirs. The ineffective flow lines were added to show water passing over the high point of the bendway weir moved from the upstream eddy to the eddy downstream of the bendway weir. The flow that passes over this portion of the bendway weir is considered ineffective since it conforms to the downstream eddy.
Trial 12	Use base-line model to build bendway weirs by using the weir option in the HEC-RAS. Look at all flow rates with the same geometry file, **NOT** independently of one another.
Trial 13	Use Trial 12 and add ineffective flow lines upstream and downstream of bendway weirs as well as at the highest elevation of the bendway weir to locate areas influenced by the eddies.
Trial 14 (8 cfs)	Use Trial 13 and change Manning's n at all cross sections with bendway weirs. Change geometry specifically for 8 cfs, model run.
Trial 14 (12 cfs)	Use Trial 13 and change Manning's n at all cross sections with bendway weirs. Change geometry specifically for 12 cfs, model run.
Trial 14 (16 cfs)	Use Trial 13 and change Manning's n at all cross sections with bendway weirs. Change geometry specifically for 16 cfs, model run.
Trial 15 (8 cfs)	Use Trial 5 (8 cfs) model and adjust contraction/expansion coefficients at cross sections in the HEC-RAS model that helps shape profile. Change geometry specifically for 8 cfs, model run.
Trial 15 (12 cfs)	Use Trial 5 (12 cfs) model and adjust contraction/expansion coefficients at cross sections in the HEC-RAS model that helps shape profile. Change geometry specifically for 12 cfs, model run.
Trial 15 (16 cfs)	Use Trial 5 (16 cfs) model and adjust contraction/expansion coefficients at cross sections in the HEC-RAS model that helps shape profile. Change geometry specifically for 16 cfs, model run.
Trial 16 (8 cfs)	Use Trial 15 (8 cfs) and adjust Manning's n and contraction/expansion coefficients simultaneously at any cross section in the HEC-RAS model that helps shape profile. Change geometry specifically for 8 cfs, model run.
Trial 16 (12 cfs)	Use Trial 15 (12 cfs) and adjust Manning's n and contraction/expansion coefficients simultaneously at any cross section in the HEC-RAS model that helps shape profile. Change geometry specifically for 12 cfs, model run.
Trial 16 (16 cfs)	Use Trial 15 (16 cfs) and adjust Manning's n and contraction/expansion coefficients simultaneously at any cross section in the HEC-RAS model that helps shape profile. Change geometry specifically for 16 cfs, model run.

NOTE: Yellow shaded cells represent trials used in analysis.

5.3 LIMITATIONS TO ANALYSIS

Limitations were placed on the analysis in order to determine if basic HEC-RAS modeling features were feasible options in developing an optimal HEC-RAS model. Basic HEC-RAS features used in the analysis were:

1. Manning's *n*;
2. contraction coefficient; and
3. expansion coefficient.

Once limitations were established, trials defined in Section 5.2 were reevaluated for the initial bendway-weir analysis. From the trial list presented in Table 5.1, seven of the sixteen defined trials were selected for this analysis. Trials selected for this bendway-weir analysis were Trial 1, Trial 2, Trial 3, Trial 4, Trial 5, Trial 15, and Trial 16. These trials are highlighted in yellow in Table 5.1.

5.4 SELECTED HEC-RAS MODEL BASED ON LIMITATIONS TO ANALYSIS

In an attempt to achieve the bendway-weir analysis goal while abiding by the limitations outlined in Section 5.3, seven of the sixteen stated trials in Table 5.1 were developed into HEC-RAS models. Of the seven trials developed into HEC-RAS models, Trial 16 was selected as the best possible HEC-RAS model.

5.4.1 Trial 16 Input Tables

During Trial 16, Manning's *n* and the contraction and expansion coefficients were adjusted simultaneously until the flow depth calculated through the HEC-RAS model

reflected flow depths measured along the physical model. Input tables for Manning's *n* and the contraction and expansion coefficients are presented in Table 5.2 and Table 5.3, respectively. In Table 5.2 and Table 5.3, W1 through W5 are interpolated cross sections in HEC-RAS that represent five bendway-weir locations in the Type I bend. W6 through W8 are interpolated cross sections in HEC-RAS that represent three bendway-weir locations in the Type III bend. Values set for Manning's *n* and the contraction and expansion coefficients did not have to reflect what is typically considered "realistic" values for these variables. Manning's *n* and the contraction and expansion coefficients were the only variables used to represent a 3-D velocity profile in a 1-D model and, therefore, values used in HEC-RAS might be greater than values typically applied to 1-D HEC-RAS models.

Table 5.2. Trial 16 Manning's *n* Values

XS	$n_{8\ cfs}$	$n_{12\ cfs}$	$n_{16\ cfs}$
0 (U/S)	0.013	0.013	0.013
W1	0.013	0.013	0.100
1	0.038	0.013	0.025
2	0.013	0.038	0.025
W2	0.013	0.013	0.090
3	0.013	0.013	0.013
W3	0.013	0.013	0.013
4	0.013	0.013	0.013
5	0.013	0.013	0.013
W4	0.013	0.013	0.013
6	0.013	0.013	0.013
7	0.013	0.013	0.013
W5	0.013	0.013	0.013
8	0.013	0.013	0.013
9	0.013	0.013	0.013
10	0.013	0.013	0.020
11	0.036	0.036	0.035
W6	0.036	0.036	0.070
12	0.023	0.023	0.023
13	0.025	0.028	0.035
W7	0.025	0.028	0.035
14	0.013	0.013	0.013
15	0.013	0.013	0.013
16	0.035	0.030	0.013
W8	0.035	0.030	0.013
17	0.013	0.030	0.013
18 (D/S)	0.013	0.013	0.013

Table 5.3. Trial 16 Expansion and Contraction Coefficients

	8 cfs		12 cfs		16 cfs	
XS	C_c	C_e	C_c	C_e	C_c	C_e
0 (U/S)	0.1	0.3	0.1	0.3	0.1	0.3
W1	0.1	0.3	0.1	0.3	0.1	0.3
1	0.1	0.3	0.1	0.3	0.1	0.3
2	0.1	0.3	0.1	0.3	0.1	0.3
W2	0.1	0.3	0.1	0.3	0.1	0.3
3	0.1	0.3	0.1	0.3	0.1	0.3
W3	0.1	0.3	0.1	0.3	0.1	0.3
4	0.1	0.3	0.1	0.3	0.1	0.3
5	0.1	0.3	0.1	0.3	0.1	0.3
W4	0.1	0.3	0.1	0.3	0.1	0.3
6	0.1	0.3	0.1	0.3	0.1	0.3
7	0.1	0.3	0.1	0.3	0.1	0.3
W5	0.1	0.3	0.1	0.3	0.1	0.3
8	0.1	0.3	0.1	0.3	0.1	0.3
9	2.5	0.3	0.1	0.3	0.1	0.3
10	4	0.3	6.8	0.3	0.1	0.3
11	5.6	0.3	7.5	0.3	3.5	0.3
W6	0.1	0.3	0.1	0.3	0.3	0.3
12	0.1	0.3	0.1	0.3	0.1	0.3
13	0.1	0.3	1.8	0.3	0.1	0.3
W7	0.1	0.3	0.1	0.3	0.1	0.3
14	0.1	0.3	0.1	0.3	0.1	0.3
15	0.1	0.3	0.1	0.3	0.1	0.3
16	0.1	0.3	4.8	0.3	0.1	0.3
W8	0.1	0.3	5.0	0.3	0.1	0.3
17	0.1	0.3	0.1	0.3	0.1	0.3
18 (D/S)	0.1	0.3	0.1	0.3	0.1	0.3

5.4.2 Trial 16 Results

Trial 16 results used HEC-RAS output for computed water-surface elevations at all cross sections marked along the physical model. Flow depth and total energy loss estimates for Trial 16 were compared to measurements collected along the physical model.

5.4.2.1 Flow-depth Comparison

Water-surface elevations along the physical model were used to calculate flow depths at each marked cross section in the physical model. Flow-depth measurements were calculated at 8 cfs, 12 cfs, and 16 cfs with Equation 4.1. Results from Equation 4.1 are presented in Table 5.4.

Table 5.4. HEC-RAS Output Flow-depth Measurements

XS	$y_{8\ cfs}$ (ft)	$y_{12\ cfs}$ (ft)	$y_{16\ cfs}$ (ft)
0 (U/S)	0.693	0.880	1.001
W1	0.702	0.890	1.007
1	0.702	0.890	1.004
2	0.719	0.907	1.018
W2	0.718	0.906	1.013
3	0.717	0.905	1.010
W3	0.726	0.913	1.018
4	0.726	0.913	1.018
5	0.715	0.902	1.007
W4	0.714	0.901	1.006
6	0.723	0.911	1.015
7	0.732	0.920	1.024
W5	0.732	0.920	1.024
8	0.741	0.929	1.032
9	0.743	0.929	1.030
10	0.697	0.915	1.009
11	0.700	0.912	1.013
W6	0.656	0.873	0.969
12	0.643	0.862	0.949
13	0.632	0.856	0.932
W7	0.621	0.847	0.896
14	0.621	0.847	0.896
15	0.613	0.843	0.889
16	0.633	0.865	0.916
W8	0.609	0.844	0.913
17	0.609	0.802	0.919
18 (D/S)	0.614	0.802	0.924

Once flow-depth calculations were completed, results were compared to flow-depth measurements along the physical model. Figure 5.1 presents flow depths calculated by HEC-RAS and measured with the track-mounted point gage for each cross section along the physical model. As Figure 5.1 illustrates, there is an abrupt increase in flow depth between XS8 and XS9. An abrupt increase in flow depth is due to the contraction between the Type I and Type III bends. The contraction creates a backwater effect which advances into the Type I bend. The backwater effect becomes less significant as the flow rate increases from 8 cfs to 16 cfs and therein, HEC-RAS is able to produce more accurate estimates of flow depth.

Cross-sectional average flow depth ($\bar{y}$) estimates in the Type I and Type III bends were calculated using the measurements presented in Table 5.4 and Figure 5.1. When calculating cross-sectional average flow depth in each bend, XS1 through XS6 were taken into account for the Type I bend and XS11 through XS17 were taken into account for the Type III bend. Cross-sectional average flow-depth results are presented in Table 5.5. As Table 5.5 shows, the cross-sectional average flow depth estimated by HEC-RAS at 8 cfs is 0.718 ft in the Type I bend and cross-sectional average flow depth measured in the physical model is 0.698 ft, which is a difference of 0.020 ft. At 16 cfs, cross-sectional average flow depth estimated by HEC-RAS is 0.929 ft in the Type III bend and cross-sectional average flow depth measured in the physical model is 0.918 ft, which is a difference of 0.012 ft. Even though the flow-depth measurements estimated by HEC-RAS did not exactly match the flow-depth measurements in the physical model, Trial 16 was still selected as the best possible HEC-RAS model given the limitations to

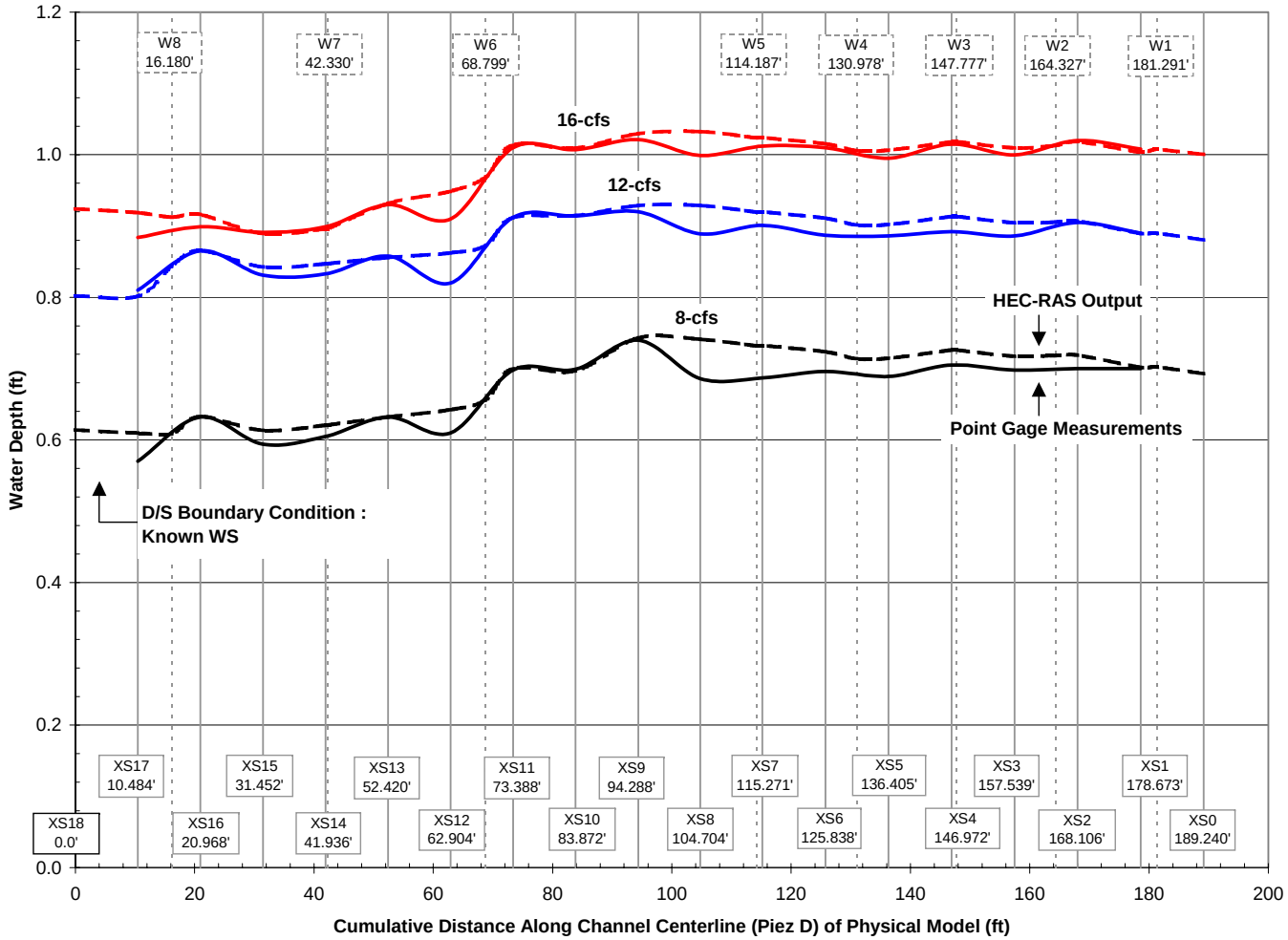

Figure 5.1. Comparison of Flow Depths Measured Along Physical Model and Estimated by HEC-RAS

the analysis. Once the flow depths were finalized, total energy and total energy loss were studied along the Type I and Type III bends.

Table 5.5. $\bar{y}$ in the Type I and Type III Bends

Bend	Physical Model Measurements			HEC-RAS Output		
	$\bar{y}_{8\ cfs}$ (ft)	$\bar{y}_{12\ cfs}$ (ft)	$\bar{y}_{16\ cfs}$ (ft)	$\bar{y}_{8\ cfs}$ (ft)	$\bar{y}_{12\ cfs}$ (ft)	$\bar{y}_{16\ cfs}$ (ft)
Type I (U/S) Bend	0.698	0.891	1.008	0.718	0.905	1.012
Type III (D/S) Bend	0.620	0.847	0.918	0.634	0.855	0.929

5.4.2.2 Trial 16 Total Energy Calculations

Total energy is calculated by summing the bed elevation, flow depth, and velocity head at a cross section. Equation 2.3 illustrated the equation used to calculate total energy at a cross section. In this analysis, total energy at each marked cross section along the physical model was calculated with physical model measurements and HEC-RAS output based on Equation 2.3. Table 5.6 presents the calculated total energy along the Type I and Type III bends using the physical model, flow-depth measurements.

Table 5.6. Total Energy Calculated With Physical Model Measurements

XS	$H_{8\ cfs}$ (ft)	$H_{12\ cfs}$ (ft)	$H_{16\ cfs}$ (ft)
0 (U/S)			
W1	97.990	98.190	98.318
1	97.953	98.147	98.270
2	97.933	98.141	98.262
W2	97.965	98.156	98.271
3	97.931	98.123	98.243
W3	97.926	98.113	98.230
4	97.928	98.119	98.247
5	97.923	98.123	98.238
W4	97.948	98.144	98.252
6	97.920	98.114	98.242
7	97.901	98.118	98.234
W5	97.916	98.128	98.240
8	97.890	98.096	98.212
9	97.937	98.123	98.232
10	97.910	98.129	98.235
11	97.889	98.107	98.217
W6	97.876	98.068	98.177
12	97.813	98.026	98.132
13	97.823	98.050	98.140
W7	97.849	98.045	98.135
14	97.789	98.017	98.103
15	97.780	98.015	98.097
16	97.783	98.016	98.075
W8	97.821	98.020	98.101
17	97.721	97.957	98.051
18 (D/S)			

Once total energy was calculated with physical model measurements, total energy was estimated with HEC-RAS output. Using the flow depths presented in Table 5.4, total energy was estimated along the physical model. Results are presented in Table 5.7. Total energy estimates throughout the physical model were used to estimate total energy loss along the Type I and Type III meander bends.

Table 5.7. Total Energy Calculated With HEC-RAS Output

XS	$H_{8\ cfs}$ (ft)	$H_{12\ cfs}$ (ft)	$H_{16\ cfs}$ (ft)
0 (U/S)	97.957	98.148	98.273
W1	97.956	98.147	98.269
1	97.955	98.146	98.266
2	97.952	98.143	98.260
W2	97.951	98.142	98.255
3	97.950	98.141	98.252
W3	97.949	98.140	98.251
4	97.949	98.140	98.251
5	97.947	98.139	98.249
W4	97.947	98.138	98.248
6	97.946	98.137	98.247
7	97.945	98.136	98.246
W5	97.945	98.136	98.245
8	97.943	98.134	98.244
9	97.941	98.132	98.241
10	97.907	98.129	98.236
11	97.892	98.108	98.222
W6	97.853	98.073	98.183
12	97.841	98.063	98.165
13	97.823	98.048	98.142
W7	97.804	98.031	98.103
14	97.803	98.030	98.102
15	97.797	98.026	98.096
16	97.784	98.017	98.090
W8	97.765	97.999	98.087
17	97.757	97.954	98.084
18 (D/S)			

5.4.2.3 Total Energy Loss Calculation

Total energy loss in an open channel system is defined as a loss of energy along a channel reach due to friction, contractions, expansions, eddies, spiral, and secondary currents. An exception to this definition is in 1-D, steady-state, gradually-varied flow analysis, where total energy loss is assumed to be due to friction, contraction, and expansion losses. Typically, contraction and expansion loss is small compared to the

friction loss and, therefore, the total energy loss is assumed approximately equal to the friction loss along a reach. In this analysis, total energy loss along the Type I and Type III bends is estimated with the EGL. The energy grade line is defined by Equation 5.1:

$$h_T = \frac{H_2 - H_1}{\Delta x} \qquad \textbf{Equation 5.1}$$

where:

Δx = distance along the centerline of the channel between cross sections (ft);

h_T = total energy loss through meander bend (ft);

H_1 = total energy at the downstream cross section (ft); and

H_2 = total energy at the upstream cross section (ft).

The EGL, also known as energy grade line slope, is used to estimate total energy loss by multiplying the EGL by the channel centerline distance. In this analysis, the EGL was calculated by plotting the total energy calculated along the Type I and Type III bends verses cumulative distance along the channel centerline and estimating the slope through linear interpolation. Using physical model measurements and HEC-RAS output, Figure 5.2 illustrates how the EGL was estimated through linear interpolation. Similar plots generated for 12 cfs and 16 cfs are presented in Appendix C.

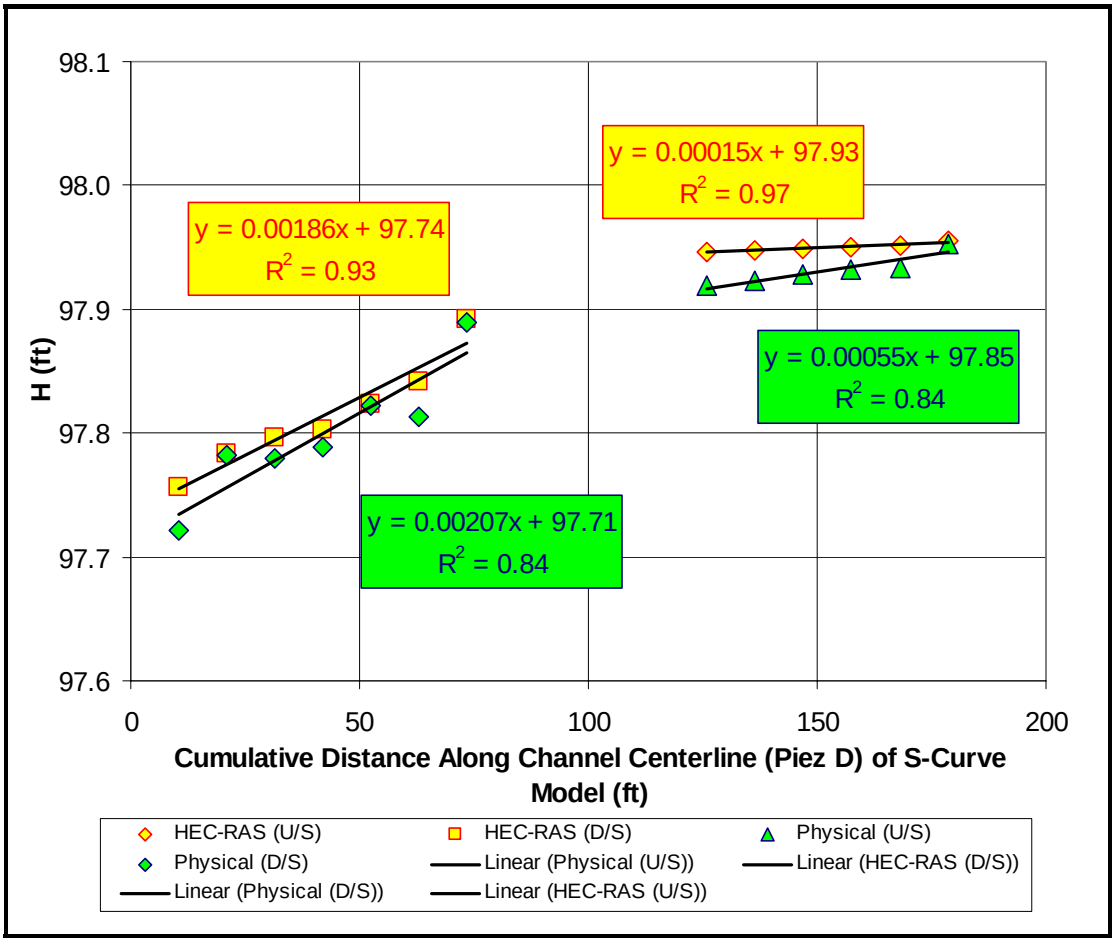

Figure 5.2. Linear Interpolation at 8 cfs

Total energy loss through a meander bend along the Type I and Type III bends was calculated with physical model measurements and HEC-RAS output. Results are presented in Table 5.8. As observed in Table 5.8, there is a significant discrepancy between total energy loss through a meander bend estimated from HEC-RAS output and the physical model measurements. The discrepancy is more significant in the Type I bend than in the Type III bend, with an average 60% difference between the actual total energy loss through a meander bend in the physical model and total energy loss through a meander bend estimated from HEC-RAS output. A possible reason for this discrepancy is the defined radius of curvature in the Type I and Type III bends. In the Type I bend,

the radius of curvature is equal to 38.75 ft and in the Type III bend, the radius of curvature is equal to 65.83 ft. As the radius of curvature tightens from the Type III bend to the Type I bend, the spiral and secondary currents become more significant and produce greater energy loss. This energy loss is evident by the comparison made in Table 5.8. Since spiral currents and secondary currents are neglected in 1-D flow computations such as HEC-RAS, additional analysis was performed to better estimate total energy loss through a meander bend through the Type I and Type III meander bends with HEC-RAS.

Table 5.8. h_T Comparison

Bend	Q (cfs)	h_T (ft) Physical Model	h_T (ft) HEC-RAS Model	Absolute Δ (%)
Type I	8	0.0291	0.0079	73
	12	0.0317	0.0085	73
	16	0.0296	0.0180	39
Type III	8	0.1302	0.1170	10
	12	0.1296	0.1233	5
	16	0.1573	0.1308	16